Brookhaven National Laboratory

BNL-229872-2026-TECH

EIC-ADD-TN-175

Machine Protection Studies of Fast Instability-Driven Beam Losses in the EIC Electron Storage Ring

A. Natochii

June 2026

Electron-Ion Collider

Brookhaven National Laboratory

U.S. Department of Energy

USDOE Office of Science (SC), Nuclear Physics (NP)

DISCLAIMER

Machine Protection Studies of Fast Instability-Driven Beam Losses in the EIC Electron Storage Ring

Andrii Natochii*
Brookhaven National Laboratory, Upton, New York 11973, USA
(Dated: June 22, 2026)

Fast transverse beam instabilities represent one of the most challenging protection scenarios for the Electron-Ion Collider (EIC) electron storage ring (ESR). Coherent betatron oscillations driven by collective effects can grow rapidly and lead to substantial beam losses within only a few tens of turns, posing a threat to collimators, superconducting (SC) magnets, cryogenic systems, and detector components.

A dedicated simulation framework based on distributed transverse excitations was developed to evaluate instability-driven beam losses in the ESR. A conservative instability rise time on the order of 10 turns was used to define a bounding protection scenario. Simulations show that the original two-collimator configuration is insufficient to localize losses under all operating conditions, whereas an optimized four-collimator configuration reduces loss leakage into protected regions by more than two orders of magnitude. Nevertheless, the most severe instability scenarios produce catastrophic beam impacts, with nearly half of the stored beam being intercepted by the collimators within a single turn, exceeding the preliminary estimated survivability limits of the baseline collimator design.

The results demonstrate that collimation alone is insufficient to guarantee safe ESR operation and must be complemented by a fast machine-protection system. Dedicated turn-by-turn beam-position monitors and fast beam-loss monitors provide sufficient advance warning to detect instability growth and initiate a beam abort before equipment-damaging loss levels are reached. These findings establish quantitative requirements for the ESR machine-protection architecture and support the implementation of a multilayer protection strategy for both accelerator and detector systems.

I. INTRODUCTION

The EIC, shown schematically in Fig. 1, will store a high-current electron beam whose total stored energy of up to 320 kJ at 10 GeV is sufficient to cause significant damage to accelerator and detector components if released in an uncontrolled manner. The combination of SC magnets, precision detector systems, and multi-ampere beam currents places stringent demands on the collimation system and machine-protection system (MPS). The ESR beam parameters relevant to the fast-instability studies reported in this paper are summarized in Table I.

Under nominal conditions, beam losses are controlled through a dedicated collimation system that intercepts beam halo and localizes unavoidable losses away from sensitive machine and detector components. However, the most demanding protection challenges do not arise from routine beam losses but from rare abnormal events capable of driving a large fraction of the stored beam into the machine aperture on extremely short timescales.

Among potential failure scenarios, fast transverse beam instabilities are particularly challenging because they can generate coherent beam losses on timescales comparable to, or even shorter than, the response time of active MPSs [2, 3]. These instabilities arise from collective effects driven by the machine impedance, which can excite coherent betatron oscillations with amplitudes that grow exponentially in time. Under collision conditions, beam-beam tune spread is expected to provide significant stabilization against transverse instabilities [4]. Additional transverse bunch-by-bunch feedback may further improve operational flexibility, particularly during commissioning, non-colliding operation, or other conditions where beam-beam stabilization is absent. If the available stabilization mechanisms are reduced or absent, coherent oscillations may grow until the beam reaches the physical aperture or collimator jaws. The resulting losses can develop within only a few tens of turns, producing highly localized energy deposition that may challenge the survivability of collimators, SC magnets, and other sensitive accelerator or detector components.

The consequences of such a failure extend beyond simple beam losses. A rapidly growing instability can simultaneously challenge several layers of machine protection. Large fractions of the beam may impact the collimator jaws before a beam abort can be completed, potentially exceeding material survivability limits. Secondary particle showers generated by these impacts can propagate downstream toward SC magnets, cryogenic systems, and experimental detector regions, where localized energy deposition may lead to magnet quenches, detector backgrounds, or in extreme cases component damage. Because instability-driven losses develop coherently rather than diffusively, their temporal evolution can be significantly faster than that associated with conventional beam-halo losses such as Touschek or beam-gas scatterings, leaving only a limited time window for protective actions.

Recent studies performed for FCC-ee [2] identified fast

* Contact author: natochii@bnl.gov

TABLE I: Ultimate EIC beam parameters used in the reported studies, adapted from Table 3.3 of Ref. [1]. The quantities β^* and $\Delta p/p$ are the betatron function at the interaction point and the fractional momentum spread, respectively.

Species	proton	electron	proton	electron	proton	electron
Energy [GeV]	275	18	275	10	100	5
Bunch intensity [10^{10}]	19.1	6.2	6.9	17.2	4.8	17.2
No. of bunches	290		1160		1160	
Beam current [A]	0.69	0.227	1	2.5	1	2.5
RMS emittance, H/V [nm]	18/1.6	24/2	11.3/1	20/1.3	26/2.3	20/1.8
RMS bunch length [cm]	6	0.9	6	0.7	7	0.7
RMS $\Delta p/p$ [10^{-4}]	6.8	10.9	6.8	5.8	9.7	6.8
β^*, H/V [cm]	80/7.1	59/5.7	80/7.2	45/5.6	61/5.5	78/7.1
Luminosity [10^{33} cm^{-2}s^{-1}]	1.54		10		3.68	

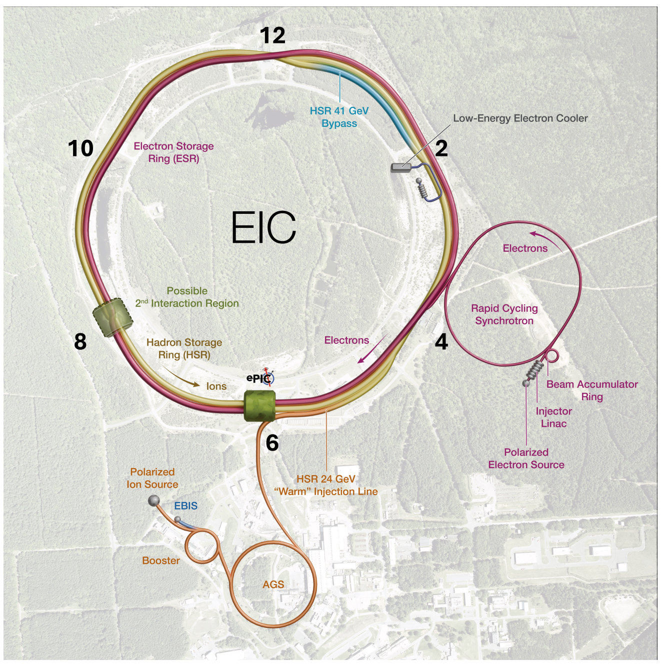

FIG. 1: Schematic layout of the EIC. The labels 2 through 12 indicate the six insertion regions (IRs) around the collider. IR6 hosts the experimental detector and adjacent SC ESR magnets, while IR4 contains the ESR collimation insertion.

coherent instabilities as one of the most challenging accidental beam-loss scenarios for future lepton colliders, demonstrating that a substantial fraction of the stored beam can be lost within only a few revolution turns. Similar concerns apply to the EIC ESR, where the final instability-mitigation strategy, including the role of beam-beam stabilization and possible feedback systems, is still under development. Consequently, understanding the development of instability-driven losses and establishing the corresponding machine-protection requirements are essential elements of the ESR design.

This work presents the first dedicated machine-protection study of fast instability scenarios in the EIC ESR. A simulation framework based on distributed transverse excitations was developed to reproduce exponentially growing coherent oscillations and evaluate the resulting beam losses using multi-turn tracking through the full ESR lattice. The study investigates realistic instability growth times, loss localization patterns, and risks to SC magnets and detector systems. Particular emphasis is placed on identifying the limiting machine-protection scenarios, evaluating the effectiveness of the ESR collimation system, and establishing requirements for diagnostics, interlocks, and beam-abort systems needed to ensure safe operation.

II. SIMULATION METHODOLOGY

The ESR is planned to begin operation at beam energies of 5 and 10 GeV, while operation at 18 GeV is currently foreseen as part of a future luminosity upgrade. Among the planned operating configurations, the 10 GeV electron beam represents the most demanding machine-protection case because it combines the highest stored beam energy in the baseline ESR operating range with the smallest protection margins for accelerator and detector components. Consequently, all studies reported in this work were performed using the 10 GeV ESR optics and beam parameters.

To evaluate the impact of fast transverse beam instabilities on the ESR collimation and MPS, a dedicated simulation framework was developed based on the methodology recently proposed for FCC-ee fast-instability studies [2]. The objective is not to model a specific impedance source in detail, but rather to reproduce the resulting coherent beam motion and quantify its consequences for beam losses, collimator survivability, and protection of sensitive accelerator and detector components.

Instead of explicitly simulating collective effects and impedance-driven beam dynamics, the instability is represented by a set of synchronized transverse dipole kickers distributed around the ESR lattice. The kickers generate coherent betatron oscillations whose amplitude grows exponentially with a prescribed rise time, reproducing the characteristic behavior expected from an unstable beam experiencing exponentially growing coherent transverse motion.

The time-dependent kicker strength is defined as

$$k_{x/y}(t) = \frac{A_0}{\sigma_{x/y}} \cos\left(2\pi Q_{x/y} t\right) e^{t/\tau}, \tag{1}$$

where $A_0 = 1 \times 10^{-12}$ m is the initial excitation amplitude, $\sigma_{x/y}$ is the local RMS beam size at the kicker location, $Q_{x/y} = 41.081/35.140$ is the horizontal or vertical betatron tune, and τ is the instability growth time. The initial amplitude was chosen sufficiently small to ensure stable beam motion during the early turns while preserving the desired exponential growth rate. Consequently, A_0 determines only the onset time of the instability and does not affect its temporal evolution.

To reproduce smooth coherent motion throughout the ring, six instability kickers per plane were installed, one in each ESR arc, as shown in Fig. 2. The reference horizontal and vertical kickers located in Arc 0 were placed such that their betatron phases matched those of the primary collimators in IR4, D04H1 and D04V1, in the horizontal and vertical planes, respectively. The remaining kickers were positioned to span a phase-advance range of approximately 90°–180° relative to the reference kicker. This configuration distributes the excitation uniformly around the ring and avoids the artificial localized excitation that would result from a single-kicker model. As a consequence, the beam centroid amplitude grows smoothly both turn-by-turn and within each revolution period, closely resembling the behavior expected from a distributed impedance source.

The kicker locations were determined by surveying the ESR lattice arc-by-arc and selecting drift sections suitable for the insertion of short, non-physical placeholder kickers. For convenience, each kicker was assigned an arbitrary length of 10 cm; the kicker length itself has no impact on the instability model since only the integrated kick strength is relevant. Figure 3 shows the distribution of kicker locations as a function of betatron phase. The selected locations reproduce the estimated target phase with excellent accuracy, yielding residual phase errors smaller than $|\Delta\mu| < 0.02 \times 2\pi$ in both transverse planes.

Particle tracking was performed using the ESR v6.3.1 lattice [5] implemented in the Xsuite framework [6]. The simulation model includes synchrotron radiation, RF cavities, collimators, beam pipe aperture restrictions, and full six-dimensional multi-turn tracking. The beam was tracked until complete loss to capture the full temporal evolution of instability-driven losses. The collimator settings ($A_{\text{coll.},1}$) defined in the dedicated studies discussed in Refs. [7, 8] are shown in Table. II.

To evaluate energy deposition and loss localization, beam-matter interactions were simulated using the Xsuite-BDSIM [9]/Geant4 [10–12] interface. Primary electrons impacting collimators were transported through realistic material models together with the resulting secondary particles. All charged secondaries ($e^{\pm}$, $\mu^{\pm}$, hadrons, and nuclear fragments) with energies above 1 GeV were further tracked through the accelerator lattice. This approach enables the evaluation of both direct beam impacts and secondary-particle showers, providing realistic estimates of energy deposition in collimators, SC magnets, cryogenic systems, and detector regions.

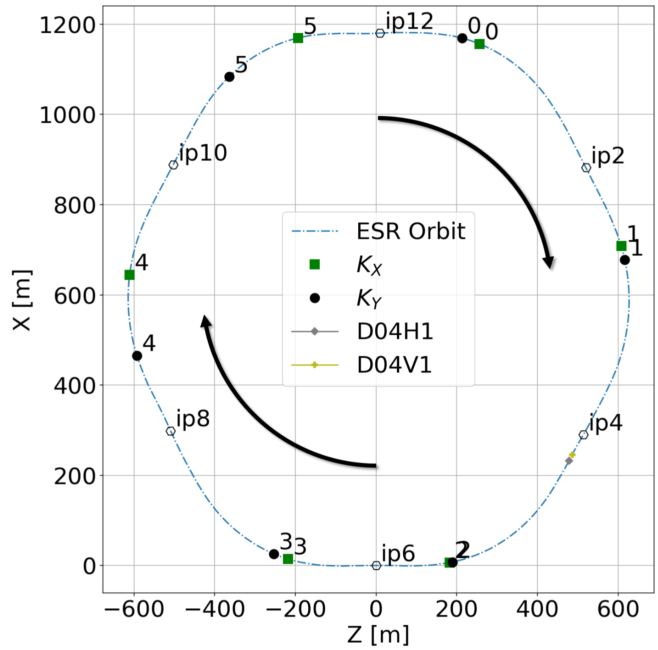

FIG. 2: Locations of the instability kickers around the ESR for the 10 GeV v6.3.1 optics. One kicker is installed in each arc to reproduce distributed coherent excitation around the ring.

TABLE II: Optics parameters and settings of the ESR collimators at 10 GeV. Here, S denotes the distance from IP6, β the betatron function, $\sigma_\beta = \sqrt{\beta\varepsilon}$ the RMS transverse beam size due to betatron motion, ε the RMS emittance, D the dispersion, and μ the betatron phase. The collimator aperture (half-opening) is indicated as $A_{\text{coll.}}$. Values are given separately for the horizontal and vertical planes, corresponding to the horizontal and vertical collimators, respectively.

Collimator Name	S [m]	β [m]	D [m]	μ [2π]	$A_{\text{coll.},1}$ [σ_β] ([mm])	$A_{\text{coll.},2}$ [σ_β] ([mm])	A_{IR6} [σ_β]
D04H1	569	83	0.1	0.03	9 (11.6)	7 (9.1)	15
D04H2	536	17	0.8	0.30	Retracted	13 (7.5)	
D04V1	585	89	0.0	0.62	21 (7.1)	19 (6.5)	28
D04V2	517	41	0.0	0.93	Retracted	20 (4.6)	

III. INSTABILITY SCENARIOS

Recent ESR impedance studies indicate that, in the event of a sudden loss of transverse damping, the fastest

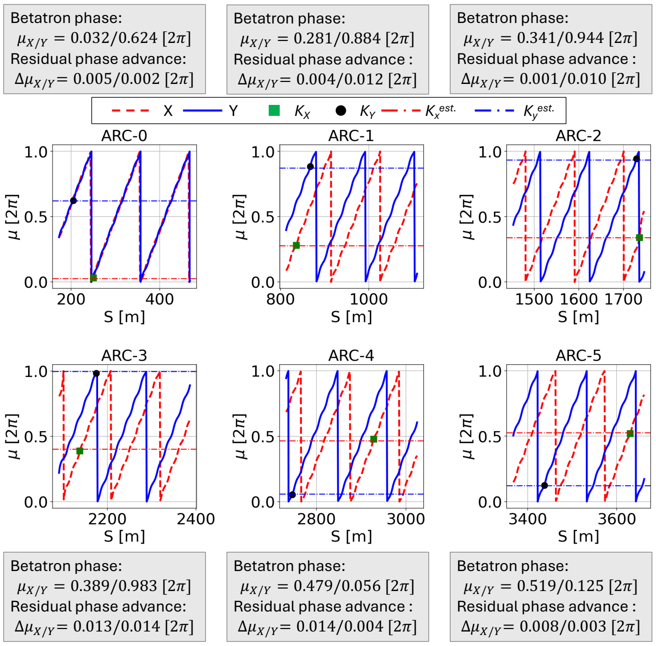

FIG. 3: Betatron phase distribution of the instability kickers. The red dashed and blue solid curves represent the horizontal and vertical betatron phase advances around the ring, respectively. Green square and black circular markers indicate the locations of the horizontal and vertical kickers. Horizontal dashed lines denote the estimated target phase advances corresponding to 0°, 90°, 112.5°, 135°, 157.5°, and 180° relative to the primary collimator.

vertical instability growth times could reach approximately 0.2 ms (about 16 turns) at 5 GeV and 0.4 ms (about 32 turns) at 10 GeV for a beam current of 2.5 A and a transverse impedance of 12 MΩ/m [13]. These estimates correspond to a pessimistic scenario in which available transverse damping is suddenly lost at full beam intensity. Under nominal operating conditions, beam-beam tune spread is expected to provide significant stabilization of transverse instabilities [4], and the actual growth rates are therefore expected to be slower.

Since the final instability-mitigation strategy and the mechanisms governing instability growth during ESR operation remain under evaluation, a broad range of instability growth times was investigated to establish bounding machine-protection requirements. A *reference growth time* of approximately 25 turns, representative of the estimates available at the time this study was initiated, was used to define the parameter scan. Conservative scenarios with significantly faster and slower instability development were then considered to assess the sensitivity of beam losses and protection performance to uncertainties in instability dynamics.

The shortest rise-time scenario was implemented as $\tau = 25/3 \approx 8.3$ turns. This value was obtained by applying a conservative factor of three relative to the reference 25-turn growth time. The scaling does not originate from a specific instability model or feedback-failure analysis and should therefore be regarded as an engineering margin introduced to evaluate machine-protection performance under substantially more severe conditions than presently expected. Consequently, the $\tau \approx 8.3$ turns case should be interpreted as a bounding scenario rather than a prediction of ESR operation.

Overall, the rise-time parameter was varied between $\tau = 25/3 \approx 8.3$ turns and $\tau = 25 \times 3 = 75$ turns. Together, these scenarios span a broad range of plausible instability conditions and provide a basis for evaluating the robustness of the ESR collimation and machine-protection systems against uncertainties in instability growth rates and stabilization mechanisms.

The parameter scan included:

- horizontal instabilities;
- vertical instabilities;
- instability growth times from approximately 10 to 75 turns;
- relative phase advances between the instability source and the primary collimator of $\Delta\mu_{\text{inst.}} = 0°$, 30°, 60°, and 90°.

The phase advance $\Delta\mu_{\text{inst.}}$ between the instability source and the collimator strongly influences the beam trajectory at the interception location and therefore affects both the loss-development rate and the resulting loss distribution around the ring. Different phase advances correspond to different beam-impact conditions, ranging from configurations in which the beam reaches the collimator aperture at relatively small oscillation amplitudes to cases where the beam bypasses the collimator during the early stages of instability growth and is instead intercepted by downstream aperture restrictions. As demonstrated in FCC-ee studies [2], such variations can significantly alter loss localization, peak energy deposition, and the effectiveness of the MPS. For this reason, a systematic scan over phase advance was performed to identify the most challenging protection scenarios and to evaluate the robustness of the ESR collimation system against uncertainties in the instability source location.

IV. MODEL VALIDATION

The validity of the instability model was verified by comparing the simulated turn-by-turn growth of the beam-centroid oscillation amplitude with the prescribed exponential growth law. The centroid amplitude was evaluated each time the beam passed the primary collimator location, corresponding to one measurement per revolution period (~ 12.8 µs).

To remove the dependence on the oscillation phase and directly quantify the instability growth, the centroid amplitude was reconstructed from the betatron action and local optics functions according to $A_{x/y} = \sqrt{2J_{x/y}\beta_{x/y}}$, where $J_{x/y}$ is the horizontal or vertical betatron action and $\beta_{x/y}$ is the corresponding betatron function at the observation point. The resulting amplitudes were then fitted using the expected instability growth law as $A_{x/y}(t) = A_0 \exp{(t/\tau)}$.

Figure 4 compares the simulated amplitudes with the fitted exponential growth curves. For the majority of the investigated scenarios, the extracted rise times are in excellent agreement with the imposed input values, demonstrating that the distributed kicker system accurately reproduces the intended instability dynamics. The level of agreement is comparable to that reported in analogous FCC-ee studies [2], providing confidence that the adopted methodology can reliably model fast instability development in the ESR and can therefore be used to evaluate collimation performance and machine-protection scenarios.

The vertical plane reaches significantly larger normalized oscillation amplitudes, $A_{x/y}/\sigma_{x/y}$, than the horizontal plane. This behavior is primarily attributed to the wider vertical collimator settings, larger available dynamic aperture [7], and smaller vertical emittance, which together allow the coherent oscillation to develop to larger amplitudes before beam interception occurs. As a result, vertical instability scenarios generally represent the more challenging machine-protection case and therefore receive particular attention in the following sections.

A noticeable discrepancy between the fitted and imposed rise times is observed for several vertical-instability scenarios with long growth times ($\tau \geq 50$ turns). The origin of this effect remains under investigation but is likely associated with physical mechanisms not included in the simplified analytical model, including synchrotron-radiation damping, nonlinear beam dynamics, amplitude-dependent tune shifts, coupling between the transverse planes, and dynamic-aperture limitations. Nevertheless, these deviations are limited to the slowest instability scenarios and do not affect the conclusions of this work, which are dominated by significantly faster growth times corresponding to the most critical machine-protection conditions.

V. LOSS LOCALIZATION AND COLLIMATION PERFORMANCE

A primary objective of the ESR collimation system is to intercept instability-driven beam losses in dedicated absorber locations and thereby prevent uncontrolled energy deposition in SC magnets, cryogenic equipment, and detector systems. To evaluate the effectiveness of the proposed collimation layout, beam-loss distributions were analyzed for all studied instability scenarios, including different growth times, instability planes, and relative phase advances between the instability source and the primary collimators.

For the majority of the investigated scenarios, beam

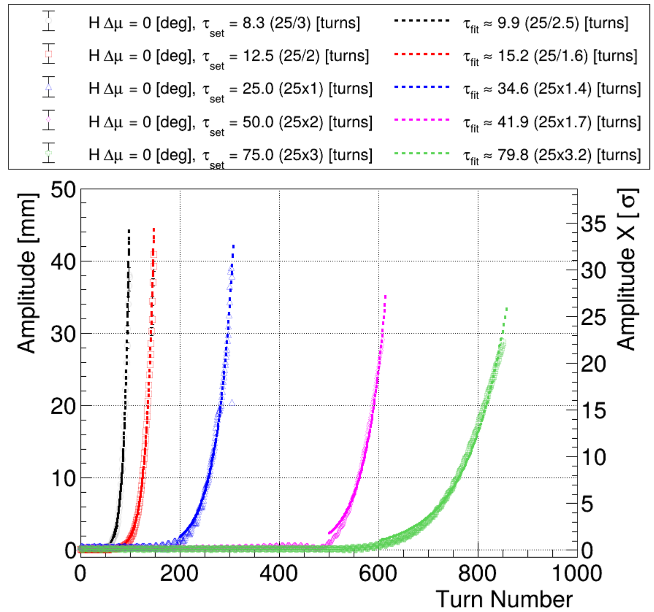

(a) Horizontal instability.

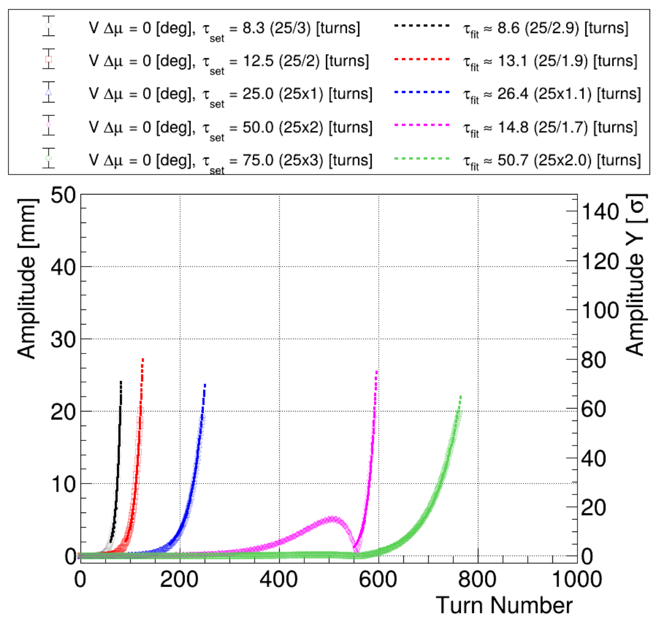

(b) Vertical instability.

FIG. 4: Evolution of the beam-centroid oscillation amplitude at the primary collimator as a function of turn number for the $\Delta\mu_{\mathrm{inst.}} = 0°$ configuration. Markers represent amplitudes reconstructed from particle tracking, while dashed curves show fits to the expected exponential growth law.

losses were successfully intercepted by the collimation system and localized in the vicinity of the primary absorbers in IR4. However, the shortest instability rise time investigated, corresponding to a growth time on the order of 10 turns, consistently produced the highest loss rates and therefore represents the limiting machine-protection scenario considered in this study. Under these conditions, the coherent oscillation develops sufficiently rapidly that a significant fraction of the beam reaches the collimator aperture within only a few tens of turns. The corresponding beam impact parameter is approximately 0.5 mm from the jaw tip, resulting in highly concentrated energy deposition and making this scenario particularly relevant for collimator survivability studies.

Initial simulations were performed using the baseline ESR configuration consisting of two primary collimators, D04H1 and D04V1 listed in Table II ($A_{\text{coll.},1}$). While this configuration provides adequate protection for many instability scenarios, it was found to be insufficient for the full range of conditions investigated. Depending on the instability plane and phase advance, a fraction of the beam can bypass the primary collimators during the early stages of oscillation growth and subsequently impact downstream aperture restrictions. As a consequence, substantial losses may occur outside the designated collimation insertion, including in the IR6 SC magnet region.

To improve loss localization and increase the robustness of the protection system, two complementary measures were implemented: tighter primary collimator settings and the inclusion of two additional collimators, D04H2 and D04V2, which are included in the current baseline ESR collimation configuration. A dedicated aperture optimization study was performed to identify settings that maximize interception efficiency while preserving acceptable beam lifetime. The resulting configuration is summarized in Table II ($A_{\text{coll.},2}$). In all cases, the optimized settings maintain beam lifetimes at the multi-hour level, fully compatible with the EIC swap-out injection scheme [1], while significantly improving loss localization.

Figure 5 compares the loss patterns obtained with the original two-collimator configuration and the optimized four-collimator configuration for the most challenging instability scenario, $\tau = 8.3$ turns and $\Delta\mu_{\text{inst.}} = 30°$. This configuration was identified as one of the most unfavorable cases because the instability phase advance reduces the effectiveness of the primary collimators during the initial stages of oscillation growth.

For horizontal instabilities, the two-collimator configuration exhibits significant uncontrolled losses outside the dedicated collimation insertion. A substantial fraction of the beam bypasses the primary absorbers and is intercepted by downstream aperture restrictions, generating losses throughout the ring and producing energy deposition in the IR6 SC magnet region approaching 10 kJ/m. Such losses are incompatible with the objective of maintaining robust protection of SC components.

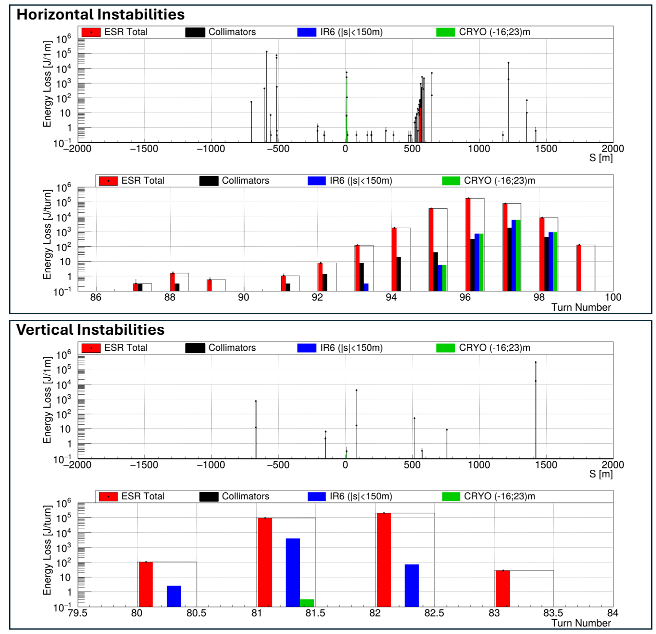

(a) Two-collimator configuration as in Table II ($A_{\text{coll.},1}$).

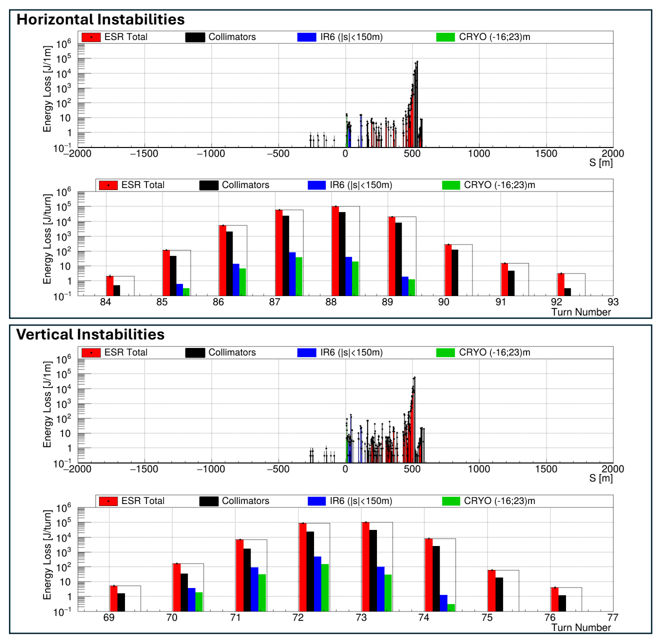

(b) Four-collimator configuration as in Table II ($A_{\text{coll.},2}$).

FIG. 5: Beam-loss distributions for the most challenging instability scenario, corresponding to $\tau = 8.3$ turns and $\Delta\mu_{\text{inst.}} = 30°$. Top panels show the integrated loss distribution around the ring, while bottom panels show turn-by-turn losses in the entire ring (red), collimators (black), IR6 region (blue), and IR6 cryostat region (green). Black markers indicate the total losses. The beam goes from right to left. The interaction point is at $S = 0$ m. Collimators are at $S \approx 500 - 600$ m.

The situation is even more severe for vertical instabilities. Owing to the larger vertical collimator aperture and larger available dynamic aperture, the beam can develop substantial coherent oscillation amplitudes before interception occurs. In the most unfavorable configurations, little or no beam interception takes place at the primary collimators, resulting in losses occurring predominantly at non-designated locations around the ring. Such loss patterns are undesirable from both machine-protection and operational perspectives because they reduce the predictability and controllability of energy deposition.

The optimized four-collimator configuration substantially improves performance in both planes. Losses become strongly localized in the IR4 collimation insertion, while leakage to downstream regions is significantly reduced. Most importantly, losses in the IR6 SC magnet region decrease by more than two orders of magnitude relative to the original configuration. Peak losses in the IR6 cryostat region remain at the level of approximately 100 J/m, and no measurable losses are observed within the detector region defined as ± 5 m around the interaction point. These results demonstrate that the baseline four-collimator configuration provides effective protection of both accelerator and detector systems even under extreme instability conditions.

The highest beam impact intensity is observed for the vertical instability with the shortest rise time. Under these conditions, nearly half of the stored beam, corresponding to approximately 580 bunches at the ultimate bunch charge of 28 nC, is intercepted by the collimators within a single revolution, producing one of the most demanding beam-impact scenarios identified in this study.

Preliminary material studies indicate that the baseline aluminum-alloy collimator design can withstand beam impacts corresponding to approximately 100 bunches at the ultimate bunch charge. The predicted instability-driven beam impact therefore exceeds the estimated survivability threshold by a factor of approximately six and cannot be considered inherently safe. These results demonstrate that absorber robustness alone is insufficient to guarantee survivability under extreme instability conditions and that rapid machine-protection intervention is required to terminate the beam before destructive impact levels are reached.

Alternative low-Z absorber concepts based on carbon-fiber composite (CFC) with conductive copper coating offer substantially improved robustness against catastrophic beam impacts and may increase survivability margins. However, these solutions require significantly longer absorber lengths, introduce additional mechanical and vacuum-design challenges, and complicate integration within the available lattice space.

The results therefore indicate that collimator survivability cannot rely solely on absorber material selection. Instead, protection against the most severe instability scenarios must be achieved through rapid machine-protection intervention capable of terminating the beam before destructive loss levels develop. Consequently, the performance of the MPS becomes at least as important as the collimator design itself for ensuring safe ESR operation.

VI. MACHINE PROTECTION REQUIREMENTS

The results presented in the previous sections demonstrate that fast transverse instabilities constitute a machine-protection challenge rather than solely a collimation problem. Although the optimized four-collimator configuration effectively localizes beam losses and substantially reduces energy deposition in protected regions, the most severe instability scenarios can still generate beam impacts that exceed the estimated survivability limits of the collimator absorbers. Furthermore, uncontrolled losses may threaten other sensitive equipment, including SC magnets, cryogenic systems, vacuum chambers, diagnostics, and detector components. Consequently, safe ESR operation requires an MPS capable of detecting instability development and initiating a beam abort before destructive losses occur.

A key result of this study is that the coherent nature of the instability provides an opportunity for predictive protection. Unlike many failure modes that are first detected through beam losses, fast transverse instabilities produce measurable orbit excursions several turns before peak energy deposition develops. These orbit excursions can be monitored using dedicated turn-by-turn beam-position monitors (BPMs) installed immediately upstream of each collimator.

Figure 6 shows the evolution of the vertical beam profile measured at a BPM located upstream of the primary vertical collimator D04V1 during instability growth. As the coherent oscillation amplitude increases, the beam centroid progressively approaches the collimator aperture of about ± 6.5 mm, providing advance warning of an impending beam impact. This information can be used to trigger a beam abort before the instability reaches a destructive level.

For the limiting instability scenario with a growth time on the order of 10 turns, corresponding to the fastest instability considered in this study, the available reaction time depends on the selected BPM threshold:

- A beam-centroid excursion exceeding $10\,\sigma$ provides approximately 4-5 turns of warning before the peak beam impact develops at the collimator.
- A more conservative threshold of $5\,\sigma$ increases the available reaction time by an additional 5-6 turns.

These warning times are particularly significant when compared with the presently estimated worst-case latency of the ESR fast-abort system, which is approximately four turns. The proposed protection chain consists of

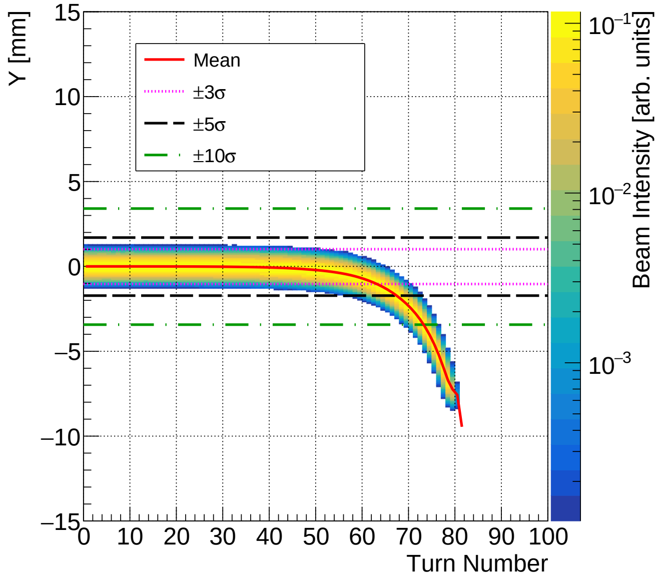

FIG. 6: Evolution of the simulated vertical beam distribution measured by the turn-by-turn BPM located immediately upstream of the primary vertical collimator D04V1 for the limiting instability scenario ($\tau = 8.3\,\text{turns}$, $\Delta\mu_{\text{inst.}} = 0°$) in the two-collimator configuration of Table II ($A_{\text{coll.},1}$). The color scale represents the normalized beam intensity, while the red curve shows the beam-centroid position. The dashed lines indicate representative MPS trigger thresholds of 3σ, 5σ, and 10σ. The progressive displacement of the beam centroid toward the collimator aperture provides several turns of advance warning before the onset of peak beam impact and associated losses.

fast sensor or equipment permit → local interlock input → deterministic abort logic → global permit removal → signal distribution → alignment with the abort gap and abort-kicker actuation → beam-safe condition.

The available warning margins therefore indicate that instability-driven beam impacts can be detected and mitigated before peak losses occur in the interaction region and collimation insertion, provided that suitable diagnostics are integrated directly into the MPS architecture.

These warning times remain comparable to or greater than the expected fast-abort latency even for the conservative bounding scenario considered in this study.

Fast beam-loss monitors (BLMs) provide a complementary and independent protection layer. During instability development, a small fraction of halo particles is expected to be intercepted before the main beam impact occurs, producing detectable loss signals several turns earlier than the onset of catastrophic losses. Fast detectors based on diamond sensors, Cherenkov detectors, or plastic scintillator-based instrumentation are expected to provide sufficient time resolution to detect these precursor losses and generate independent abort requests. Such redundancy is particularly valuable because it reduces dependence on any single diagnostic system and increases overall protection reliability.

The proposed protection strategy is therefore based on the combined use of orbit and loss diagnostics. Turn-by-turn BPMs provide predictive information by directly monitoring coherent oscillation growth, while fast BLMs provide confirmation through the observation of early particle losses. Together, these systems establish multiple independent paths for initiating a beam abort before dangerous loss levels are reached.

Based on the results of this study, each ESR collimator location is planned to be equipped with:

- at least one dedicated turn-by-turn BPM installed immediately upstream of the absorber;
- at least one fast (turn-by-turn or better) beam-loss monitor integrated directly into the MPS interlock chain.

It is important to emphasize that the objective of this instrumentation is not limited to protecting the collimators themselves. The primary purpose is to prevent instability-driven beam losses from reaching vulnerable accelerator and detector systems, including SC magnets, cryogenic equipment, vacuum components, and experimental detectors. In this sense, the collimators serve as the first line of defense, while the MPS provides the final protection layer that prevents abnormal beam conditions from evolving into equipment-damaging events.

The present results therefore establish quantitative requirements for the ESR machine-protection architecture. Specifically, the MPS must be capable of identifying coherent orbit excursions and abnormal loss patterns within only a few turns and initiating a beam abort before instability-driven losses exceed the survivability limits of either the collimation system or other protected machine components.

VII. LIMITATIONS AND FUTURE WORK

The results presented in this study provide a first comprehensive assessment of fast instability scenarios in the EIC electron storage ring and their implications for collimation and machine protection. Nevertheless, several limitations should be considered when interpreting the results and defining future work.

First, the instability is represented by externally imposed coherent transverse kicks rather than by a fully self-consistent impedance model. This approach was intentionally adopted to reproduce the characteristic exponential growth of the coherent oscillation while maintaining computational efficiency and direct control of the instability rise time. Although it successfully reproduces the desired instability dynamics and provides a realistic framework for machine-protection studies, it does not capture the detailed underlying collective effects, nonlinear beam-impedance interactions, bunch-by-bunch feedback dynamics, or possible changes in instability behavior at large oscillation amplitudes.

The present study focuses on the consequences of rapidly growing coherent transverse beam motion. The dominant operational instability in the ESR may originate from different physical mechanisms, including longitudinal multibunch effects. Consequently, the results should be interpreted as a study of beam-loss consequences and machine-protection requirements rather than a prediction of a specific ESR instability mode.

Second, the present study focuses primarily on beam-loss localization and absorbed energy at the lattice-tracking level. While these quantities provide a useful measure of relative risk, they are not sufficient for evaluating equipment survivability. Dedicated Geant4 energy-deposition simulations are required to determine local energy-density distributions in collimators, SC magnets, cryogenic systems, vacuum components, and detector infrastructure. Such studies are particularly important for evaluating quench margins of SC magnets and for establishing realistic damage thresholds for accelerator components.

Third, uncertainties remain regarding the final ESR instability-mitigation strategy and the mechanisms that will ultimately determine instability growth rates during operation. Future studies should incorporate realistic impedance models, beam-beam stabilization effects, and, if implemented, transverse feedback-system dynamics including damping performance, signal-processing delays, gain limitations, saturation effects, and representative failure scenarios. Such simulations would allow a more accurate determination of instability growth rates under both nominal and abnormal operating conditions.

Fourth, the present simulations were performed using the ideal ESR lattice and therefore do not include several important machine features that may influence instability development, loss localization, and machine-protection performance. In particular, future studies should incorporate the detector solenoid field, crab cavities, realistic magnet misalignments, magnetic-field errors, orbit distortions, optics correction residuals, and other machine imperfections expected during operation. These effects can modify beam trajectories, dynamic aperture, collimation hierarchy, and loss distributions, and are therefore required for a fully realistic assessment of machine-protection margins.

Finally, the current work evaluates the machine-protection requirements based on available warning times inferred from beam dynamics simulations. A complete assessment will require an end-to-end MPS model that includes turn-by-turn BPMs, fast BLMs, interlock logic, signal transmission delays, abort-gap synchronization, kicker rise times, beam extraction dynamics, and beam-dump performance. Such a model would enable direct verification that the full protection chain can respond within the available time window identified in this study.

Despite these limitations, the present work establishes a conservative framework for evaluating instability-driven beam losses and identifying machine-protection requirements. In particular, the shortest rise-time scenario considered should be interpreted as a conservative machine-protection bounding case rather than a prediction of expected ESR operation. The methodology provides a foundation for future studies incorporating increasingly realistic machine models and protection-system implementations.

VIII. CONCLUSIONS

A dedicated simulation framework has been developed to investigate fast transverse instability scenarios in the EIC electron storage ring and evaluate their implications for beam-loss localization, collimator survivability, and machine protection. Adapted from recent FCC-ee studies, the methodology reproduces exponentially growing coherent oscillations using distributed transverse excitations and enables realistic modeling of instability-driven beam losses throughout the ESR.

The simulations demonstrate that fast transverse instabilities constitute one of the most demanding machine-protection scenarios for ESR operation. Depending on the instability growth rate and source location, a substantial fraction of the stored beam can be lost within only a few tens of turns, producing highly localized energy deposition in collimators and potentially exposing SC magnets, cryogenic systems, and detector components to uncontrolled losses.

The shortest rise-time scenario investigated, corresponding to a conservative instability growth time on the order of 10 turns, was identified as the limiting protection case. For the original two-collimator configuration, significant beam losses were observed outside the designated collimation insertion, including substantial energy deposition in the IR6 SC-magnet region. The addition of the baseline collimators D04H2 and D04V2, together with optimized collimator settings, significantly improves loss localization. The resulting four-collimator configuration confines losses to the IR4 collimation insertion and reduces leakage into protected regions by more than two orders of magnitude.

Despite the significantly improved collimation performance, the most severe instability scenarios result in nearly half of the stored beam being intercepted by the collimators within a single turn. This exceeds the preliminary estimated survivability limits of the baseline aluminum-alloy collimator design by a substantial margin. These results demonstrate that optimized collimation alone cannot guarantee safe ESR operation and must be complemented by a fast MPS capable of detecting instability growth and initiating a beam abort before destructive beam impacts occur.

A key outcome of this work is the identification of predictive protection signatures. Turn-by-turn BPMs installed upstream of the collimators can detect coherent orbit excursions several turns before peak beam impact develops, while fast BLMs provide an independent confirmation channel through the observation of precursor losses. For the limiting scenario, BPM-based thresholds provide warning times comparable to or exceeding the expected fast-abort latency, indicating that instability-driven beam losses can be mitigated before equipment-damaging conditions are reached.

This study therefore establishes the need for a multi-layer protection strategy consisting of optimized collimation, dedicated turn-by-turn BPMs, fast BLMs, and a low-latency beam-abort system. Together, these systems provide protection not only for the collimators themselves, but also for SC magnets, cryogenic equipment, vacuum components, and detector infrastructure.

The shortest rise-time scenario considered in this work should be interpreted as a conservative bounding case rather than a prediction of expected ESR instability performance. A more realistic assessment of instability growth rates will require detailed modeling of ESR impedance sources, beam-beam stabilization effects, and any future feedback-system implementation. Future studies will incorporate these effects, together with detector-solenoid and crab-cavity fields, machine imperfections, detailed Geant4 energy-deposition calculations, and end-to-end simulations of the machine-protection chain to further refine protection margins and support safe ESR operation.

ACKNOWLEDGMENTS

The authors thank their colleagues in the EIC Project for valuable discussions and continuous support of this work. In particular, we gratefully acknowledge B. Podobedov and M. Blaskiewicz (BNL) for valuable discussions of transverse beam instabilities and feedback-system performance, for providing instability growth-time estimates used to define the simulation scenarios investigated in this study, and for their careful review of the manuscript, which helped improve its technical accuracy and clarity.

We also acknowledge the Jefferson Lab Scientific Computing Team for providing access to the JLab computing farm, which enabled the large-scale, CPU-intensive simulations required for this work.

This work was supported by the U.S. Department of Energy under Contract No. DE-SC0012704.

[1] F. Willeke and J. Beebe-Wang, Electron Ion Collider Conceptual Design Report 2021, Tech. rep., BNL-221006-2021-FORE; TRN: US2215154 (2021). doi:10.2172/1765663.

[2] G. Nigrelli, et al., Simulations of Losses from Fast Instabilities in the FCC-ee, in: Proceedings of IPAC'25, 2025.

[3] M. Migliorati, E. Belli, M. Zobov, Impact of the resistive wall impedance on beam dynamics in the future circular e+e- collider, Phys. Rev. Accel. Beams 21 (2018) 041001.

[4] J. Qiang, M. Blaskiewicz, Strong–strong simulations of combined beam–beam and wakefield effects in the Electron–Ion-Collider, Nucl. Instrum. Methods Phys. Res. A 1069 (2024) 169942. doi:https://doi.org/10.1016/j.nima.2024.169942. URL https://www.sciencedirect.com/science/article/pii/S0168900224008684

[5] Y. Nosochkov *et al.*, Dynamic aperture studies for the EIC electron storage ring, JACoW IPAC2025 (2025) MOPS135. doi:10.18429/JACoW-IPAC2025-MOPS135.

[6] G. Iadarola *et al.*, Xsuite: An Integrated Beam Physics Simulation Framework, JACoW HB2023 (2024) TUA2I1. arXiv:2310.00317, doi:10.18429/JACoW-HB2023-TUA2I1.

[7] A. Natochii, E.-C. Aschenauer, K. Hamdi, C. Hetzel, E. Link, D. Marx, C. Montag, S. Tepikian, Y. Cai, Y. Nosochkov, Collimation system baseline design for the electron storage ring at the Electron-Ion Collider, Phys. Rev. Accel. Beams (Jun 2026). doi:10.1103/2v68-np87. URL https://link.aps.org/doi/10.1103/2v68-np87

[8] A. Natochii, Thermal Compton Scattering of Electron Beams on Blackbody Photons: A Monte Carlo Event Generator for Multi-Turn Tracking at the Electron-Ion Collider, Tech. rep. (02 2026). doi:10.2172/3021706. URL https://www.osti.gov/biblio/3021706

[9] L.J. Nevay *et al.*, BDSIM: An accelerator tracking code with particle–matter interactions, Comput. Phys. Commun. 252 (2020) 107200. doi:https://doi.org/10.1016/j.cpc.2020.107200. URL https://www.sciencedirect.com/science/article/pii/S0010465520300400

[10] S. Agostinelli *et al.*, Geant4 — a simulation toolkit, Nucl. Instrum. Methods Phys. Res., Sect. A 506 (3) (2003) 250–303. doi:https://doi.org/10.1016/S0168-9002(03)01368-8. URL https://www.sciencedirect.com/science/article/pii/S0168900203013688

[11] J. Allison *et al.*, Geant4 developments and applications, IEEE Trans. Nucl. Sci. 53 (1) (2006) 270–278. doi:10.1109/TNS.2006.869826.

[12] J. Allison *et al.*, Recent developments in Geant4, Nucl. Instrum. Methods Phys. Res., Sect. A 835 (2016) 186–225. doi:https://doi.org/10.1016/j.nima.2016.06.125. URL https://www.sciencedirect.com/science/article/pii/S0168900216306957

[13] M. Blaskiewicz, private communication, 2026.